The Journal of Physiology

Image-based assessment of microvascular function and structure in collagen XV- and XVIII-deficient mice

C. B. Rygh[1,5], G. Løkka[1], R. Heljasvaara[2], T. Taxt[1], T. Pavlin[1], R. Sormunen[3], T. Pihlajaniemi[2], F. R. Curry[4], O. Tenstad[1] and R. K. Reed[1,6]

[1] *Department of Biomedicine, University of Bergen, Norway*
[2] *Oulu Center for Cell-Matrix Research, Biocenter Oulu and Department of Medical Biochemistry and Molecular Biology, Institute of Biomedicine, University of Oulu, and Oulu University Hospital, Oulu, Finland*
[3] *Biocenter Oulu and Departments of Pathology, University of Oulu, and Oulu University Hospital, Oulu, Finland*
[4] *Department of Physiology and Membrane Biology, University of California, Davis, CA 95616, USA*
[5] *The Cardiovascular Research Group, Haukeland University Hospital, Bergen, Norway*
[6] *Center for Cancer Biomarkers (CCBIO), University of Bergen, Norway*

Key points

- Collagen XV and XVIII occur in muscle and connective tissue capillaries and are needed for maintaining a normal circulatory phenotype.
- Lack of collagen XV in mice leads to increased vascular permeability, increased extraction fraction, and increased extravascular extracellular space in striated muscle.
- Lack of collagen XVIII in mice leads to increased blood flow, permeability, permeability–surface area product and blood–tissue transvascular transfer in striated muscle tissue.
- Our results show that functional imaging with MRI and subsequent data analysis provide reliable and robust data and are valuable tools for assessing detailed physiological information non-invasively.

Abstract Collagen XV and XVIII are ubiquitous constituents of basement membranes. We aimed to study the physiological roles of these two components of the permeability barrier non-invasively in striated muscle in mice deficient in collagen XV or XVIII by dynamic contrast-enhanced magnetic resonance imaging (DCE-MRI). Structural information was obtained with transmission electron microscopy (TEM). MR data were analysed by two different analysis methods to quantify tissue perfusion and microcirculatory exchange parameters to rule out data analysis method-dependent results. Control mice (C57BL/6J Ola/Hsd strain) or mice lacking either collagen XV (*Col15a1*$^{-/-}$) or XVIII (*Col18a1*$^{-/-}$) were included in the study. MR images were acquired using a preclinical system using gadodiamide (Gd-DTPA-BMA, molecular weight 0.58 kDa) as a tracer. Exchange capacity (permeability (*P*)–surface area (*S*) product relative to blood flow (F_B)) was increased in test mice compared to controls, but the contributions from *P*, *S*, and F_B were different in these two phenotypes. F_B was significantly increased in *Col18a1*$^{-/-}$, but slightly decreased in *Col15a1*$^{-/-}$. *PS* was significantly increased only in *Col18a1*$^{-/-}$ even though *P* was increased in both phenotypes suggesting *S* might also be reduced in *Col15a1*$^{-/-}$ mice. Immunohistochemistry and electron microscopy demonstrated alterations in capillary density and morphology in both knockout mouse strains in comparison to the control mice. Both collagen XV and XVIII are important for maintaining normal capillary permeability in the striated muscle. DCE-MRI and the perfusion analyses successfully determined microvascular

C. B. Rygh and G. Løkka contributed equally to this work.

DOI: 10.1113/jphysiol.2013.263574

haemodynamic parameters of genetically modified mice and gave results consistent with more invasive methods.

(Received 20 August 2013; accepted after revision 4 November 2013; first published online 11 November 2013)
Corresponding author C. B. Rygh: Department of Biomedicine, University of Bergen, Jonas Lies vei 91, 5009 Bergen, Norway. Email: cecilie.rygh@biomed.uib.no

Abbreviations ANP, atrial natriuretic peptide; BM, basement membrane; CNV, choroidal neovascularization; DCE-MRI, dynamic-contrast-enhanced magnetic resonance imaging; E, extraction fraction; EES, extravascular extracellular space; ROI, region of interest; SI, signal intensity; TEM, transmission electron microscopy.

Introduction

In recent years, our understanding of the vascular basement membranes (BMs) has changed dramatically, from being mere structural components of tissues and barriers to infiltration to acting as an active modulator of blood vessel formation and function, including the properties of the microcirculatory exchange barrier (Sund *et al.* 2004). The vascular BM of normal blood vessels is a uniform, well-defined sheet-like extracellular matrix underlying the endothelial cell layer and separating the endothelial cells from the stroma. It serves as an anchor for the pericytes and provides the vessels additional structural support (Kalluri, 2003; Sund *et al.* 2004). The BM surrounding the blood vessels also contributes to sequestering growth factors and angiogenic factors which influence the vasculature. The molecular composition characteristic of vascular BMs differs to some extent from the epithelial BMs (Kalluri, 2003) and there are also differences between the BMs of different vessels (Myllyharju & Kivirikko, 2004). The major components of the vascular BM include collagen IV, laminin, and proteoglycans which assemble to form a tight network that serves as a scaffold for endothelial cells (Kalluri, 2003; Sund *et al.* 2004). Collagen XV and XVIII are common constituents of most endothelial and epithelial BMs. The continuous capillaries, found in all muscular and connective tissues, have BMs containing both of these collagens (Tomono *et al.* 2002). Collagen XVIII has structural properties typical of collagens, which includes several non-collagenous domains, and also a proteoglycan with attached heparan sulphate side-chains. The closely related collagen XV is also glycosylated, with chondroitin-sulphate side-chains attached to a collagenous core protein (Iozzo, 2005). Together, collagen XV and XVIII form a distinct multiplexin group within the collagen superfamily (Myllyharju & Kivirikko, 2004) and their proteolytically cleaved C-terminal parts, named restin and endostatin are classified as endogenous angiogenesis inhibitors (Sund *et al.* 2004; Iozzo, 2005).

Although these two types of collagen are structurally closely related, they appear to be functionally independent, with collagen XV prevalent in skeletal muscle and heart and collagen XVIII in the eye. Studies with knockout mice have shown that collagen XV is necessary for the structure and proper function of microvessels in the skeletal muscle, heart and in the skin (Eklund *et al.* 2001; Tomono *et al.* 2002; Rasi *et al.* 2010). On the other hand, mice lacking collagen XVIII have eye abnormalities and defects in the vasculature of the eye (Fukai *et al.* 2002; Marneros & Olsen, 2005). In addition, abnormally broadened BMs have been observed in kidney proximal tubules, heart valves, epidermis and choroid plexus of collagen XVIII-deficient mice (Utriainen *et al.* 2004). These observations indicate that this collagen is important for the structural integrity and function of endothelial and epithelial BMs (Utriainen *et al.* 2004).

Our hypothesis was that the circulatory phenotypes are dependant on the presence of collagen XV and/or collagen XVIII. We estimated blood volume, permeability, permeability–surface area products, extraction fraction (fraction of tracer removed from plasma in one vascular passage) and extracellular extravascular volume in knockout mice lacking either collagen XV (*Col15a1*$^{-/-}$ mice) or collagen XVIII (*Col18a1*$^{-/-}$ mice) using dynamic contrast-enhanced MRI (DCE-MRI) and subsequent perfusion analysis. Two different pharmacokinetic methods for analysis of perfusion properties were used in order to eliminate methods-dependent results. MR imaging methods may provide important information on the functional properties of the microcirculation both in healthy and diseased organs, are non-invasive so repeated studies of the same animal can be performed, and have a great translational value. We have recently reported a method (step–slope model) to determine the permeability of the capillary wall of a high molecular weight tracer using the initial tracer uptake in skin and skeletal muscle of mice lacking the atrial natriuretic peptide (ANP) receptor on endothelial cells (Curry *et al.* 2010). The other perfusion analysis method using single-channel blind deconvolution with the adiabatic approximation model of Johnson and Wilson has been used to quantify capillary permeability, extraction fraction, extracellular extravascular volume and redistribution of the tracer back to the vasculature, as well as blood flow, blood volume and intravascular transit time in a region of interest (Taxt *et al.* 2012). The present investigations are the first detailed application of this blind deconvolution approach in mouse models of altered microvascular function and are a step towards fulfilling the need for new non-invasive ways to study the regulation of microvascular exchange in whole animal tissues.

Our new findings demonstrate that the striated muscle in mice lacking collagen XV or mice lacking collagen XVIII have increased blood-to-tissue leakage of a low molecular weight tracer although the relative contributions of increased perfusion and increased vascular permeability to the increased clearance differ between the two phenotypes. Light and electron microscopic analyses revealed abnormalities in the capillary density and ultrastructure of the capillaries in the knockout masseter muscle, which at least partially can explain the observed functional differences detected by MRI.

Methods

Ethical approval

All animal procedures were performed in accordance with protocols approved by The National Animal Research Authority (Oslo, Norway), and the investigation conforms to the *Guide for the Care and Use of Laboratory Animals* published by the US National Institutes of Health (NIH Publication No. 85–23, revised 1996).

Mice

Adult (10–12 weeks old) female mice deficient in collagen XV (*Col15a1*$^{-/-}$; Eklund *et al.* 2001) or collagen XVIII (*Col18a1*$^{-/-}$; Fukai *et al.* 2002), both backcrossed for at least 15 times to the C57BL/6J OlaHsd strain, were used in these studies ($n = 10$ for *Col15a1*$^{-/-}$ and *Col18a1*$^{-/-}$; $n = 9$ for control). Female mice from the C57BL/6J OlaHsd strain (Harlan, The Netherlands) served as control animals. The mice were anaesthetized with 3.5% isoflurane (Isoba vet, Intervet Schering-Plough Animal Health, Middlesex, UK) for induction and maintained with 1.5–2% isoflurane in air supplied via a nose cone. The animals were monitored continuously for respiratory rate (i.e. 60–80 breaths min^{-1}) and body temperature ($37 \pm 0.2^{\circ}$C).

Tracer

The low-molecular weight gadolinium-based contrast agent Omniscan (gadodiamide, molecular weight 0.58 kDa, GE Healthcare, Oslo, Norway) was used as a tracer for DCE-MRI.

Magnetic resonance imaging

MR imaging was performed using a horizontal bore 7T Bruker Pharmascan 70/16 (Bruker Biospin MRI, Ettlingen, Germany) with a dedicated mouse bed and a mouse head coil. Dynamic MRI data were obtained with a T1-weighted FLASH (Fast Low Angle Shot) pulse sequence with a flip angle of 25 deg, and repetition time (TR) and echo time (TE) of 11.1 and 2.5 ms, respectively. A total of 1200 images were acquired with a sampling interval of 0.795 s (total scan time 16 min) and slice thickness of 1 mm. The field of view was 3.5 cm and the acquisition matrix was 96×96, giving an image pixel resolution of 0.364×0.364 mm. The contrast agent (0.1 mmol (kg BW)$^{-1}$, diluted 1:4 in saline) was injected over 10 s through a catheter in the tail vein after acquisition of 30 baseline images. The signal intensity (SI) over time was followed before, during and after injection. T1-maps and proton density maps needed for estimation of perfusion parameters were generated from six T1-weighted images with a fixed TR and TE (same as in the dynamic sequence) and with flip angles of 5, 10, 15, 20, 25 and 30 deg.

Regions of interest and estimation of microvascular parameters

Regions of interest including the upper part of the deep masseter muscle were carefully drawn on MR images. The masseter muscle was chosen because it is a relatively large muscle and is not affected by respiratory motion artifacts. The mouse head was fixed using a tooth bar and tape. No movements were observed in all animals for left and right masseter muscle or whole head using time frame video inspection and no time series co-registration of images was therefore needed. Eight of the collagen XV and three of the collagen XVIII data sets had artifacts in the ventral–dorsal direction (phase-encoding direction) due to movement of the tongue larger or equal to one pixel during the time sequence. The movement of the tongue did not cause artifacts in the left and right muscle masseter region. Perfusion parameters were estimated from the dynamic image data using two different perfusion analysis methods. The step–slope model is previously described in detail (Curry *et al.* 2010), and is a simplified version of the Tofts' model (Tofts, 1997; Tofts *et al.* 1999). It has two independent parameters and assumes a fixed intravascular/extravascular volume fraction. The second method uses single-channel blind deconvolution with the adiabatic approximation model of Johnson and Wilson (aaJW model; Johnson & Wilson, 1966; Taxt *et al.* 2012), which is also called the adiabatic approximation tissue homogeneity pharmacokinetic model, and includes both an intravascular and an extravascular extracellular compartment. We made the assumption that 1 ml of tissue is equivalent with 1 g of the same tissue.

Perfusion analysis using the step–slope model

The apparent solute permeability was estimated using the step–slope method (Curry *et al.* 2010). The signal intensity curves in muscle tissue and large vessels were obtained using nordicICE version 2.3.5 (Nordic Image Control and Evaluation, NordicNeuroLab AS, Bergen, Norway). A

linear relationship was assumed between signal intensity and tracer concentration (Curry *et al.* 2010). The arterial input was achieved by measuring the signal intensity in large arteries close to the region of interest (ROI), and the half-life of the tracer in blood was calculated in order to take into account the tracer exchange to the interstitium. This analysis is based on initial tracer uptake. The controlled injection of the tracer caused an initial step increase in signal intensity due to vascular filling, subsequently followed by an initial linear increase (slope) in tracer concentration in the tissue for about 30 s. The rate of increase of tissue tracer concentration is an estimate of transvascular tracer flux into the region of interest after a measured increase (i.e. step of the curve) in vascular tracer concentration. An initial estimate of the apparent solute permeability was calculated from the slope and step assuming a microvessel volume-to-surface ratio of 4.4 μm (Curry *et al.* 1983, 2010).

Perfusion analysis using the aaJW pharmacokinetic model

This analysis is based on the whole tracer signal, i.e. both the tracer uptake and tracer clearance from the tissue. This analysis was performed using a new single-channel blind deconvolution method with in-house software written in C, based on the Xite image processing software from University of Oslo, Norway and further described by Taxt and coworkers (Taxt *et al.* 2012). In blind deconvolution, both the arterial input function and the tissue residual function are estimated from the observed tissue contrast function (Gruner & Taxt, 2006). Using the blind approach avoids common problems such as delay, dispersion and partial volume effects since only the integral of the arterial input function is needed as input to the blind algorithm in addition to the observed tissue tracer function. The integral estimation is noise-robust and reliable, and its value is easily estimated from a large artery or vein. This new algorithm estimates primarily blood flow, transit time, extraction fraction and the time constant of the exponential decay of the tracer washout from the tissue. From these four independent parameters, blood volume, extracellular volume and the permeability–surface area product are then calculated (Taxt *et al.* 2012).

Histochemical and immunohistochemical analyses

The deep masseter was harvested from the three different genotypes at the age of 3 months ($n = 2$ per genotype). The tissue samples were fixed with 4% paraformaldehyde and embedded in paraffin. Endothelial cells were identified using a marker for CD31, which is a glycoprotein expressed on endothelial cells. Five micrometre tissue sections were dewaxed and stained either with Haematoxylin and Eosin (H&E) or with a rat anti-mouse CD31 antibody (BD Biosciences PharMingen, San Diego, CA, USA) using a colour-intensifying tyramide signal amplification method (PerkinElmer, Waltham, MA, USA) as described previously (Rasi *et al.* 2010). Images were captured with a Leica DM LB2 microscope digital camera system (Leica Microsystems, Wetzlar, Germany) and processed using Leica IM50 software. Capillary densities in the masseter muscle and images of the CD31-stained cross-sections (22–25 images per genotype) were quantified with ImageJ software (The National Institutes of Health, Bethesda, MD, USA).

Transmission electron microscopy

Masseter muscle samples ($n = 2$ per genotype) were fixed for 12 h with 1% glutaraldehyde and 4% paraformaldehyde in 0.1 M phosphate buffer, pH 7.4. The specimens were postfixed in 1% osmium tetroxide, dehydrated in acetone and embedded in Epon LX 112 (Ladd Research Industries, Vermont, NE, USA). Sections 1 μm thick were stained with Toluidine Blue for histological analysis, and 80 nm sections were cut with a Leica Ultracut UCT microtome, and examined in a Philips CM100 transmission electron microscope (TEM). Images were captured with a Morada CCD camera (Olympus Soft Imaging solutions GMBH, Munster, Germany).

Statistical methods

Comparisons between groups were made using one-way ANOVA with *post hoc* Bonferroni or Holm-Sidak tests. When comparing two groups only, two-tailed *t* tests were used, and $P < 0.05$ was considered statistically significant. SPSS 16.0 software was used for the statistical calculations of capillary density and a two-tailed *t* test was used to determine statistical significance.

Results

Based on the signal intensity curves obtained with DCE-MRI in large vessels (see Fig. 1*A*), the half-life of the tracer was estimated and used for further calculations of permeability. The half-life of Omniscan was not statistically different between the groups and individual values for each animal were used. The values ranged between 80 and 120 s. The signal intensity *versus* time curves from the ROI in the deep masseter muscle revealed altered pharmacokinetics, reflected in different slopes, time to peak, peaks and wash-out slopes of the tracer in the striated muscle of the different genotypes (Fig. 1*B*). Representative MR images from animals in each group during the baseline, peak and clearance phase (Fig. 1*C*) demonstrate a uniform distribution throughout the deep masseter muscle within the same time frame, indicating

that the results are not due to noise but to differences in microvascular function, i.e. that the depletion of collagen XV or collagen XVIII induced an altered circulatory phenotype compared to the control animals. Quantitative assessment of perfusion parameters presented below confirmed the qualitative evaluation of differences in the circulatory phenotype.

Analysis based on initial tracer uptake

The differences in the initial tracer accumulation visualized as different slopes in Fig. 1 were confirmed when estimating the permeability coefficients. The solute permeability was significantly increased in both knockout strains compared to the control animals, i.e. $8.8 \pm 2.3 \times 10^{-6}$ cm s^{-1} for control mice and 16.0 ± 3.2 and $13.4 \pm 3.0 \times 10^{-6}$ cm s^{-1} for the *Col15a1*$^{-/-}$ and *Col18a1*$^{-/-}$ groups, respectively (Table 1). No differences were identified between populations from the left and right masseter muscles (Fig. 2). In control mice the correlation between left and right permeability estimates was $r = 0.72$ (Pearson analysis), indicating that in the absence of other sources of variation, duplicate measurements on the same animal were internally consistent.

Analysis based on whole tracer signal

Both tracer-non-specific (blood flow, blood volume, transit time and extravascular extracellular space (EES)) and tracer-specific parameters were estimated using the blind deconvolution method (Table 1). Blood flow in the *Col15a1*$^{-/-}$ mice was slightly decreased but not significantly changed compared to controls (i.e. 15.5 ± 3.4 and 17.7 ± 6.6 ml (100 g)$^{-1}$ min^{-1}, respectively), while blood flow was significantly increased (24.5 ± 8.2 ml (100 g)$^{-1}$ min^{-1}) in the *Col18a1*$^{-/-}$ mice ($P < 0.05$). Blood volume was in the range of 2.5–2.8 ml (100 g)$^{-1}$ tissue in all three groups while EES was calculated at 25.7 ± 7.4 and 25.2 ± 4.9 ml (100 g)$^{-1}$

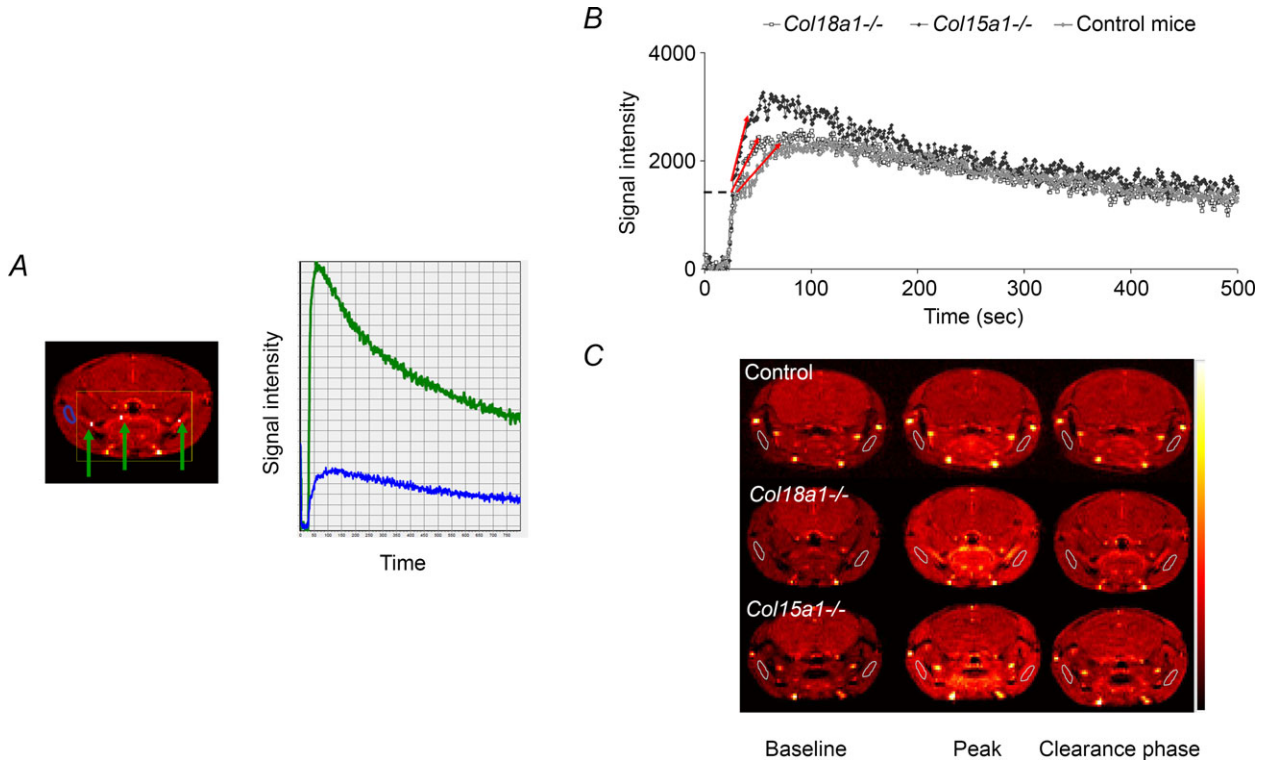

Figure 1. Signal intensity curves and MR images
A, on the right signal intensity curvesfrom larger vessels (green curve) demonstrate the typical time-course of an arterial input curve. A typical SI curve of muscle tissue (blue curve) is shown in the same graph for comparison. Larger vessels are identified as high intensity regions (green arrows, left). *B*, representative registrations of signal intensity *versus* time curves from mice in the three groups: control, *Col15a1*$^{-/-}$ and *Col18a1*$^{-/-}$ mice. The dashed line marks the step, which is caused by vascular filling. The red arrows indicate the slope of the curves, which represents the tracer accumulation. *C*, dynamic MR images (pseudocoloured) of representative animals from each group, acquired at different time-points, i.e. baseline before injection, at the peak signal intensity and in the late clearance phase. The muscle ROIs are delineated by white lines and were manually drawn on both sides to include larger parts of the muscle.

Table 1. Estimated vascular parameters from DCE-MRI data (means ± SD)

Model parameter (unit)*	Control ($n = 9$)	*Col15a1*$^{-/-}$ ($n = 10$)	*Col18a1*$^{-/-}$ ($n = 10$)
Permeability ($\times 10^{-6}$ cm s^{-1})	8.8 ± 2.3	16.0 ± 3.2†	13.4 ± 3.0†
Blood flow (ml (100 g)$^{-1}$ min^{-1})	17.7 ± 6.6	15.5 ± 3.4	24.5 ± 8.2
Blood volume (ml (100 g)$^{-1}$)	2.7 ± 0.7	2.8 ± 0.6	2.8 ± 0.6
Transit time (s)	10.5 ± 4.8	11.2 ± 2.6	7.3 ± 1.9
Extraction fraction	0.53 ± 0.05	0.65 ± 0.02†	0.59 ± 0.07
Blood flow × extraction (ml (100 g)$^{-1}$ min^{-1})	9.2 ± 3	9.9 ± 1.9	14.1 ± 4.0†
PS product (ml (100g)$^{-1}$ min^{-1})	9.7 ± 3.1	11.6 ± 2.5	15.4 ± 4.4†
PS/blood flow (min^{-1})	0.55 ± 0.03	0.71 ± 0.03†	0.65 ± 0.03†
K^{trans}	6.8 ± 2.3	7.1 ± 1.33	10.2 ± 2.9†
Extracellular volume (ml (100 g)$^{-1}$)	25.7 ± 7.4	18.3 ± 3.4†	25.2 ± 4.9
k_{ep}	0.37 ± 0.07	0.55 ± 0.06†	0.56 ± 0.13†

*Permeability values in first row were estimated with the step–slope model, whereas the other vascular parameters were estimated using the single channel blind deconvolution and the adiabatic approximation tissue homogeneity model. †$P < 0.05$ compared to control.

in control and in *Col18a1*$^{-/-}$ mice, respectively, but was significantly less in *Col15a1*$^{-/-}$ mice (18.3 ± 3.4 ml (100 g)$^{-1}$, $P < 0.05$).

Tracer-specific parameters such as the extraction fraction (E) increased significantly from 0.53 ± 0.05 in control mice to 0.65 ± 0.02 in *Col15a1*$^{-/-}$ mice ($P < 0.05$, Table 1). The extraction fraction in mice lacking collagen XVIII was 0.59 ± 0.07, which is not significantly different compared to control or *Col15a1*$^{-/-}$ mice. Together, all the above results indicate different contributions of changes in blood flow and permeability to the exchange capacity of the microcirculation of the two knockout models. An estimate of these different contributions was made using the following further analysis of the results.

The permeability–surface area (*PS*) products calculated from the measured extraction and blood flow demonstrated that the *PS* product in *Col18a1*$^{-/-}$ mice increased significantly when compared to the control (Table 1; 15.4 *vs.* 9.7 ml (100 g)$^{-1}$ min^{-1}; $P < 0.05$). However, the *PS* product in *Col15a1*$^{-/-}$ mice was not as large as expected from the significantly increased extraction fraction and did not reach statistical significance (Table 1). This may be explained if some increase in the measured extraction was due to reduced blood flow but the extent of the increase was offset by reduced surface area for exchange.

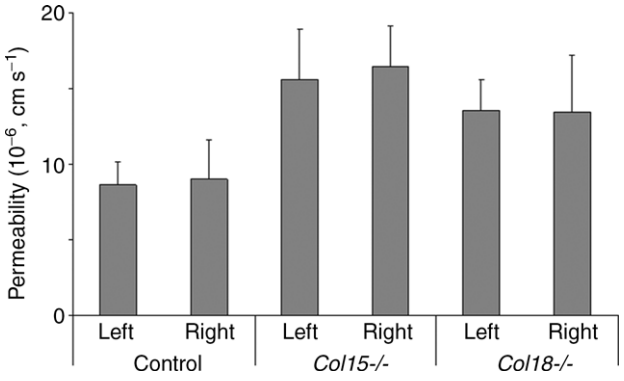

Figure 2. Permeability analysis with the step-slope method
Permeability analysis using the step–slope model of the right and left masseter muscle in the same experiment ($\times 10^{-6}$ cm s^{-1}, mean ± SD). No statistical differences were seen group-wise between the right and left masseter in the same strains.

Another way to express the contribution of changes in permeability and blood flow (F_B) in the two phenotypes relative to control is to note the ratio of PS/F_B (exchange capacity relative to solute delivery). This ratio was 0.55 ± 0.03 in control animals and was significantly increased in both knockouts (0.71 ± 0.03 and 0.65 ± 0.03 for *Col15a1*$^{-/-}$ and *Col18a1*$^{-/-}$, respectively). In addition, blood–tissue transvascular transfer is typically denoted K^{trans}, which approximates *PS* when $PS \ll F_B$, i.e. the depletion of the tracer from blood is permeability limited and not flow limited (Tofts *et al.* 1999). K^{trans} was significantly increased in *Col18a1*$^{-/-}$ muscle tissue compared to control mice and *Col15a1*$^{-/-}$. The rate constant describing transvascular transport from tissue to blood, k_{ep} (the ratio K^{trans}/EES), was also significantly larger for *Col15a1*$^{-/-}$ than the other groups.

Thus, both methods to determine microcirculatory exchange properties based on DCE-MRI clearly suggest that the transvascular exchange capacity is increased in skeletal muscle of both *Col15a1*$^{-/-}$ and *Col18a1*$^{-/-}$ mice.

Ultrastructure of microvessels

Histological examination of Haematoxylin–Eosin stained masseter specimens by light microscopy did not reveal visible alterations in the overall tissue or vessel morphology between the mutant and control mice (data not shown). This is not surprising in view of the high resolution required to observe detailed changes in

microvessels. Thus in order to correlate the functional findings with the underlying capillary morphology in the masseter muscle of the *Col15a1*$^{-/-}$ and *Col18a1*$^{-/-}$ mice, we analysed the ultrastructure of the capillary wall by transmission electron microscopy. TEM images demonstrated that in control mice the capillaries had normally shaped endothelial cells and formed capillaries with an open lumen, a compact and uniform vascular BM and well-defined endothelial cell–cell junctions (Fig. 3*A* and *D*). In contrast, capillaries in the C*ol15a1*$^{-/-}$ and *Col18a1*$^{-/-}$ mice showed several abnormalities. Uneven and degenerated endothelia and protrusions of the endothelium towards lumen were frequent findings in the C*ol15a1*$^{-/-}$ masseter (Fig. 3*B*). In the C*ol18a1*$^{-/-}$ mice malformed capillaries with swollen endothelium and narrowed lumen were often seen (Fig. 3*C*). In addition, capillaries in both mutant mouse strains were often filled with residues, probably representing degenerated endothelial cells (Fig. 3*B* and *C*). The vascular BM was abnormally broadened in C*ol18a1*$^{-/-}$ mice, whereas it appeared normal in C*ol15a1*$^{-/-}$ mice (Fig. 3*D*–*F*). An interesting observation was the occurrence of less prominent endothelial cell–cell junctions often seen focally in the C*ol15a1*$^{-/-}$ mice but not to the same extent in the C*ol18a1*$^{-/-}$ or control mice (Fig. 3*D*–*F*).

Immunohistochemical staining with CD31 showed that the masseter capillary density was significantly higher in the two types of knockout mice compared with the controls, the average being 308 ± 56 capillaries per field in control mice, and 349 ± 48 and 350 ± 82 capillaries per field in *Col15a1*$^{-/-}$ and *Col18a1*$^{-/-}$ mice, respectively (Fig. 4).

Discussion

Collagen modulation of transvascular exchange

Functional data obtained by DCE-MRI demonstrate that the exchange capacity of the microvasculature in skeletal muscle is dependent on the expression of collagen XV and XVIII. A vascular defect measured as increased transvascular tracer transport was present in *Col15a1*$^{-/-}$ mice as well as in *Col18a1*$^{-/-}$ mice. Collagens XV and XVIII are associated with most vascular BMs, including the capillaries of striated muscle (Hagg *et al.* 1997; Saarela *et al.* 1998; Eklund *et al.* 2001; Tomono *et al.* 2002), and thus the increase in transvascular exchange most likely reflects defects in the endothelial barrier of these mice. Ultrastructural analysis of the capillaries using TEM supported this conclusion but suggested that increased leakage is via different mechanisms in the two phenotypes.

The TEM images of mice deficient in collagen XV demonstrated a reduced endothelial barrier with degenerated endothelial cells and weakened cell–cell junctions. The pathway via inter-endothelial junctions is a major determinant of transvascular exchange and a reduction in intercellular junction resistance may cause increased vascular extraction fraction and permeability. Our current findings further support the earlier observations on the crucial role of collagen XV in stabilizing microvessels. Previous studies revealed collapsed capillaries, endothelial cell degeneration and swelling in the heart and skeletal muscle, the sites of the highest collagen XV expression (Eklund *et al.* 2001). Additional defects in the *Col15a1*$^{-/-}$ hearts included tortuous capillaries varying in thickness, frequent ruptures

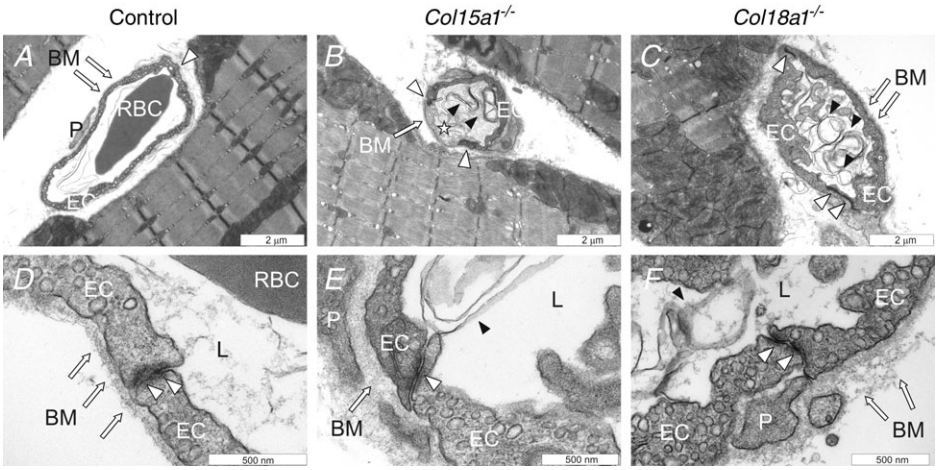

Figure 3. Capillary morphology and endothelial cell–cell junctions in the masseter muscle
Representative transmission electron micrographs of capillaries of control animals (*A* and *D*), *Col15a1*$^{-/-}$ (*B* and *E*) and *Col18a1*$^{-/-}$ mice (*C* and *F*). TEM micrographs of two mice per genotype were evaluated. Arrows point to endothelial basement membrane, white arrowheads to endothelial cell–cell junctions and black arrowheads to endothelial cell residues. Star indicates a degenerated endothelial cell. EC = endothelial cell; BM = basement membrane; P = pericyte; L = capillary lumen.

in the capillary walls and extravasated erythrocytes (Rasi *et al.* 2010). However, the capillaries showed normal pericyte coverage, indicating normal maturation of the vessels in the absence of collagen XV. Intravital microscopy has also revealed microvascular dysfunction (increased permeability, decreased capillary perfusion index, reduced blood cell velocity and lower microvascular blood flow rate) in the skin of the *Col15a1*$^{-/-}$ mice (Rasi *et al.* 2010).

In *Col18a1*$^{-/-}$ mice the capillary permeability was increased, which is reflected in increased *PS* product and K^{trans}. TEM showed that the cell–cell junctions of the *Col18a1*$^{-/-}$ capillaries did not have major defects and were comparable to those of the control animal capillaries, and thus the increased *PS* product and K^{trans} are most probably due to the abnormalities in the BM structure and/or endothelial cells. Our results correspond well with previous reports that mice lacking collagen XVIII expression manifest developmental defects in retinal and hyaloid vasculature (Fukai *et al.* 2002), increased vascular leakage from the retinal capillaries during (laser-induced) choroidal neovascularization (CNV; Marneros *et al.* 2007), as well as enhanced vascular permeability in the small vessels of the skin and in atherosclerotic aorta (Moulton *et al.* 2004). We have also shown previously that wound capillary density is increased in *Col18a1*$^{-/-}$ mice (Seppinen *et al.* 2008). In the present study of *Col18a1*$^{-/-}$ mice, both muscle blood flow and capillary density detected with CD31 immunohistochemistry were increased and contributed to increased exchange. These observations together imply that collagen XVIII has multiple roles as a determinant of transvascular exchange and vascular development.

Comparison to other microvascular data

Data for skeletal muscle blood flow in mice are scarce but the values obtained in the present study compare well with two studies in mouse skeletal muscle reporting on average 27 ml (100 g)$^{-1}$ min^{-1} for mixed skeletal muscle (Wang *et al.* 1993) and 1 ml g^{-1} min^{-1} in quadriceps (Cardinal & Hoying, 2007). Also, measurements of blood flow in C57BL/6 mice using MRI has given average values of 0.9 ml g^{-1} min^{-1} (Streif *et al.* 2003), increasing to 1.8 ml g^{-1} min^{-1} after vasodilatation with adenosine. The calculated data for extracellular volume and plasma volume in skeletal muscle compare well to our previous data reported on skeletal muscle (Aukland & Reed, 1993).

The present value of *PS* for the tracer with a molecular weight of 0.58 kDa in control mice, 9.7 ml (100 g)$^{-1}$ min^{-1}, is comparable with data for

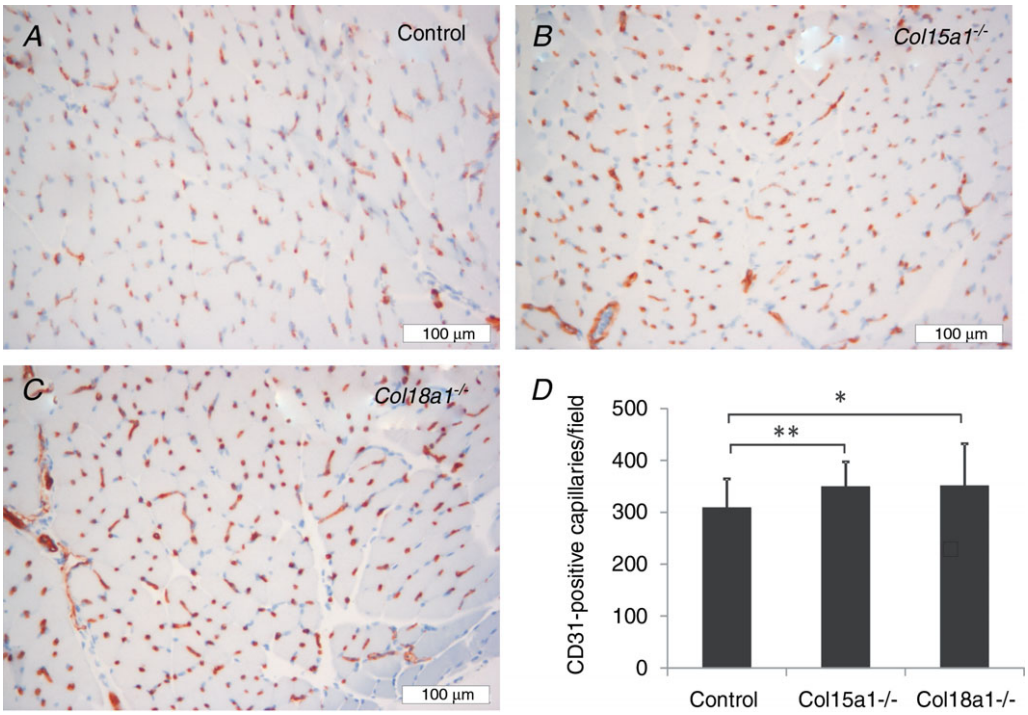

Figure 4. Masseter muscle capillary density
Representative images of the CD31-positive capillaries in the masseter muscle of the C57BL/6 control (*A*), *Col15a1*$^{-/-}$ (*B*) and *Col18a1*$^{-/-}$ (*C*) mice. *D*, quantification of the CD31-positive capillaries. Mean ± SD capillary densities in control ($N = 2$, $n = 22$), *Col15a1*$^{-/-}$ ($N = 2$, $n = 25$) and *Col18a1*$^{-/-}$ mice ($N = 2$, $n = 24$). N = number of mice; n = number of fields analysed; $^{*}P < 0.05$; $^{**}P < 0.01$.

PS values for sucrose (0.34 kDa) reported for skeletal muscle (mainly hindlimb in cats, dogs, or rats; 3–7.2 ml (100 g)$^{-1}$ min^{-1}) (Crone & Lewitt, 1984). If we assume that the surface areas available for exchange in mouse skeletal muscle are similar to those in other mammals (50–200 cm^2 g^{-1}) the *PS* of gadodiamide in control animals corresponds to solute permeability coefficients of 8 to 30 $\times$ 10^{-6} cm s^{-1}. The control values for permeability estimated from the step–slope method (8.8 $\times$ 10^{-6} cm s^{-1}) also fall in the range estimated for sucrose which range from 5.4 to 13.5 $\times$ 10^{-6} cm s^{-1} using the indicator diffusion method while higher values are obtained using residue detection, compartmental analysis or venous outflow technique (Crone & Lewitt, 1984). Because extraction increased when blood flow also increased, a true increase in *PS* product was indicated. Thus, the data presented here using non-invasive DCE-MRI is in line with our previous observations on leaky vasculature in the muscle of the *Col15a1*$^{-/-}$ mice.

However, direct comparison of microvascular parameters achieved by various methods is complicated due to the physiological effects of different anaesthetics. Here we used the volatile agent isoflurane mixed with air to study the perfusion of striated muscle tissue. The physiological effect of isoflurane is dose dependent and has been extensively studied by several groups. Isoflurane preserves cardiac function better than other anaesthetics such as urethane, pentobarbital, and ketamine/xylazine (Berry *et al.* 2009), but may cause a mild reduction of left ventricular systolic function compared with conscious animals (dose 0.6–2.2%; Takuma *et al.* 2001). Several studies have reported that isoflurane causes vasodilatation and increased capillary blood flow, especially in doses above 2% (Kober *et al.* 2004). However, Baudelet & Gallez (2004) reported that in isoflurane-anaesthetized mice, they observed no differences in hindlimb muscle perfusion using laser Doppler ultrasound scanning and 1.5% isoflurane. In this study, the dose of isoflurane was regulated (1.5–2%) based on physiological observations such as respiration rate in order to achieve stable and comparable conditions for all animals in all groups. However, a potential increased effect of muscular blood flow may have occurred. If so, a similar effect would be expected in all groups and would not explain the group differences we observed.

The strengths and weaknesses of the methods

The current resolution of our MRI system (0.364 $\times$ 0.364 mm in plane at acquisition time of 0.795 s) cannot resolve either individual capillaries (mean diameter in the order of 4–5 μm) nor venular microvessels (mean diameter up to 30 μm). Increasing the number of image elements will also increase the sampling time, giving a poorer temporal resolution. Thus, rather than measuring the properties of the individual capillary, the current methodology measures the combined function of microvessels in a unit (voxel) of tissue. The ideal situation would be a method that enables measurements at both the single capillary and at tissue voxel level, but current MRI resolution is not at this level. However, the advantage with the MRI technique is that it is atraumatic, although it does require a brief anaesthesia and intravenous injection of the tracer substance. Further, the MRI method allows repeated measures in the same tissue and microvascular bed days and weeks apart, each completed over a short recording time. These are features that are much more difficult when studying isolated and perfused capillaries.

The functional MRI data were analysed using two perfusion analysis methods to confirm that the estimated changes in microvascular physiology were based on the underlying biology and not dependent of the applied methodology. The step–slope method has been applied previously for DCE-MRI data using a high molecular weight tracer (35 kDa; Curry *et al.* 2010) whose permeability coefficients were more than one order of magnitude smaller ($PS/F_B < 0.1$) than using small molecular weight tracers. When using a high molecular weight tracer, the conditions are not flow limited but permeability limited, which removes the effect of blood flow on the estimated permeability parameters (Curry & Adamson, 2010; Curry *et al.* 2010). Because estimates of PS/F_B fall in the range of 0.55–0.71 in the present experiments, changes in blood flow that contributed to estimated increased tracer accumulation would be interpreted in terms of increased permeability and likely overestimates the contribution of increased permeability to increased transvascular exchange.

The heterogeneity of microvascular blood flow caused by capillary endothelial dysfunction may also partly account for the estimate of a larger increase in the permeability in *Col15a1*$^{-/-}$ mice relative to control using the step–slope method compared with the analysis based on the whole time course of the tracer signal. For example, the initial part of the signal intensity curve may be weighted by well-perfused regions of the muscle microvascular bed of *Col15a1*$^{-/-}$ mice whereas the later part of the curve may be preferentially weighted by regions with lower flow. In the latter analysis the effect of flow heterogeneity is likely to be amplified because of the non-linear relation between extraction fraction and flow.

The volume-to-surface area ratio (V/S) of 4.4 μm used for step–slope analyses was calculated previously as a weighted average characteristic of microvessels less than 60 μm in diameter in a masseter muscle ROI. The weighting was based on the typical vessel size and number within a normal skeletal muscle (50% venular vessels ($V/S = r/2 = 7.5$ μm and 50% capillaries, $V/S = r/2 = 1.25$ μm). The limited new data from both histology and ultrastructure in the current investigations

provided no clear way to modify the estimates of the volume to surface ratio in test *Col15a1*$^{-/-}$ and *Col18a1*$^{-/-}$. For example, the tendency for this ratio to decrease when partially collapsed vessels were taken into account (as in some *Col15a1*$^{-/-}$ muscles as seen in Fig. 3) would be offset by the increased microvessel density (Fig. 4). While a much more detailed ultrastructural analysis could provide a more accurate estimate of the volume-to-surface ratio for each test tissue, the approach does not appear warranted. This is because the consistency between the results of the step–slope analysis (which weights the early part of the tracer exchange) and the more detailed kinetic analysis of the whole tracer curve indicates that both approaches provide a reasonable index of real changes in permeability despite change in microvessel architecture that may also be present.

The power of a more detailed analysis is illustrated by the observations that the significantly increased blood flow in *Col18a1* $^{-/-}$ mice had to be taken into account when interpreting the modest increase in tracer extraction. If *PS* had remained constant while blood flow alone increased, extraction would have decreased. If *PS* had increased only in proportion to increased perfused surface, extraction would have remained constant. Similarly, the more detailed analysis suggests that the measured significant increase in the tracer peak in *Col15a1*$^{-/-}$ mice cannot be attributed solely to increased permeability coefficient because muscle blood flow was slightly decreased relative to controls.

However, it is noted that a detailed understanding of changes in microvascular function often also requires measurement of changes in permeability to high molecular weight compounds. For example, low molecular weight tracers are not particularly sensitive to changes in the selectivity of the microvessel wall. There can be large changes in the permeability of the vascular wall to plasma proteins such as albumin with only small changes in permeability to low molecular weight tracers. In many cases the tissue extraction of the larger tracer may be too small to reliably apply the blind deconvolution method. Thus, further understanding of defects in microvascular exchange function such as those described above may be best investigated using a combination of both methods. Given the increasing number of mouse models of disturbed microvascular exchange function, we suggest that the approaches used in the present investigations may have quite wide applicability.

Summary

Physiological data obtained with DCE-MRI revealed altered microvascular function in *Col15a1*$^{-/-}$ and *Col18a1*$^{-/-}$ mice, indicating important roles of collagen XV and collagen XVIII in maintaining the vessel wall integrity. Alterations in the structure or integrity of endothelial BM lead to increased vascular fragility and permeability, and substantially contribute to diverse functions of the vessels and compromise the microcirculation. Our results extend our understanding of the roles of collagen XV and XVIII in maintaining and regulating the capillary permeability, which has not been studied previously. DCE-MRI and subsequent data analyses as employed in this study provided reliable and robust data that lead to improved characterization of the circulatory phenotypes of *Col15a1*$^{-/-}$ and *Col18a1*$^{-/-}$ mice. Also, since MR perfusion imaging is done *in vivo*, repeated measurement over time can be used to study the time course of the development of vascular dysfunction, and the effectiveness of treatment.

References

Aukland K & Reed RK (1993). Interstitial-lymphatic mechanisms in the control of extracellular fluid volume. *Physiol Rev* **73**, 1–78.

Baudelet C & Gallez B (2004). Effect of anaesthesia on the signal intensity in tumors using BOLD-MRI: comparison with flow measurements by Laser Doppler flowmetry and oxygen measurements by luminescence-based probes. *Magn Reson Imaging* **22**, 905–912.

Berry CJ, Thedens DR, Light-McGroary K, Miller JD, Kutschke W, Zimmerman KA & Weiss RM (2009). Effects of deep sedation or general anaesthesia on cardiac function in mice undergoing cardiovascular magnetic resonance. *J Cardiovasc Magn Reson* **11**, 16.

Cardinal TR & Hoying JB (2007). A modified fluorescent microsphere-based approach for determining resting and hyperemic blood flows in individual murine skeletal muscles. *Vascul Pharmacol* **47**, 48–56.

Crone C & Lewitt DG (1984). *Handbook of Physiology: The Cardiovascular System*. Sect. 2, vol IV, Ch 10, pp. 411–466. American Physiological Society, Bethesda, MD, USA.

Curry FE, Huxley VH & Adamson RH (1983). Permeability of single capillaries to intermediate-sized colored solutes. *Am J Physiol Heart Circ Physiol* **245**, H495–H505.

Curry FR & Adamson RH (2010). Vascular permeability modulation at the cell, microvessel, or whole organ level: towards closing gaps in our knowledge. *Cardiovasc Res* **87**, 218–229.

Curry FR, Rygh CB, Karlsen T, Wiig H, Adamson RH, Clark JF, Lin YC, Gassner B, Thorsen F, Moen I, Tenstad O, Kuhn M & Reed RK (2010). Atrial natriuretic peptide modulation of albumin clearance and contrast agent permeability in mouse skeletal muscle and skin: role in regulation of plasma volume. *J Physiol* **588**, 325–339.

Eklund L, Piuhola J, Komulainen J, Sormunen R, Ongvarrasopone C, Fassler R, Muona A, Ilves M, Ruskoaho H, Takala TE & Pihlajaniemi T (2001). Lack of type XV collagen causes a skeletal myopathy and cardiovascular defects in mice. *Proc Natl Acad Sci U S A* **98**, 1194–1199.

Fukai N, Eklund L, Marneros AG, Oh SP, Keene DR, Tamarkin L, Niemela M, Ilves M, Li E, Pihlajaniemi T & Olsen BR (2002). Lack of collagen XVIII/endostatin results in eye abnormalities. *EMBO J* **21**, 1535–1544.

Grüner R & Taxt T (2006). Iterative blind deconvolution in magnetic resonance brain perfusion imaging. *Magn Reson Med* **55**, 805–815.

Hagg PM, Hagg PO, Peltonen S, Autio-Harmainen H & Pihlajaniemi T (1997). Location of type XV collagen in human tissues and its accumulation in the interstitial matrix of the fibrotic kidney. *Am J Pathol* **150**, 2075–2086.

Iozzo RV (2005). Basement membrane proteoglycans: from cellar to ceiling. *Nat Rev Mol Cell Biol* **6**, 646–656.

Johnson JA & Wilson TA (1966). A model for capillary exchange. *Am J Physiol* **210**, 1299–1303.

Kalluri R (2003). Basement membranes: structure, assembly and role in tumour angiogenesis. *Nat Rev Cancer* **3**, 422–433.

Kober F, Iltis I, Izquierdo M, Desrois M, Ibarrola D, Cozzone PJ & Bernard M (2004). High-resolution myocardial perfusion mapping in small animals *in vivo* by spin-labelling gradient-echo imaging. *Magn Reson Med* **51**, 62–67.

Marneros AG & Olsen BR (2005). Physiological role of collagen XVIII and endostatin. *FASEB J* **19**, 716–728.

Marneros AG, She H, Zambarakji H, Hashizume H, Connolly EJ, Kim I, Gragoudas ES, Miller JW & Olsen BR (2007). Endogenous endostatin inhibits choroidal neovascularization. *FASEB J* **21**, 3809–3818.

Moulton KS, Olsen BR, Sonn S, Fukai N, Zurakowski D & Zeng X (2004). Loss of collagen XVIII enhances neovascularization and vascular permeability in atherosclerosis. *Circulation* **110**, 1330–1336.

Myllyharju J & Kivirikko KI (2004). Collagens, modifying enzymes and their mutations in humans, flies and worms. *Trends Genet* **20**, 33–43.

Rasi K, Piuhola J, Czabanka M, Sormunen R, Ilves M, Leskinen H, Rysa J, Kerkela R, Janmey P, Heljasvaara R, Peuhkurinen K, Vuolteenaho O, Ruskoaho H, Vajkoczy P, Pihlajaniemi T & Eklund L (2010). Collagen XV is necessary for modeling of the extracellular matrix and its deficiency predisposes to cardiomyopathy. *Circ Res* **107**, 1241–1252.

Saarela J, Rehn M, Oikarinen A, Autio-Harmainen H & Pihlajaniemi T (1998). The short and long forms of type XVIII collagen show clear tissue specificities in their expression and location in basement membrane zones in humans. *Am J Pathol* **153**, 611–626.

Seppinen L, Sormunen R, Soini Y, Elamaa H, Heljasvaara R & Pihlajaniemi T (2008). Lack of collagen XVIII accelerates cutaneous wound healing, while overexpression of its endostatin domain leads to delayed healing. *Matrix Biol* **27**, 535–546.

Streif JU, Hiller KH, Waller C, Nahrendorf M, Wiesmann F, Bauer WR, Rommel E & Haase A (2003). *In vivo* assessment of absolute perfusion in the murine skeletal muscle with spin labelling MRI. Magnetic resonance imaging. *J Magn Reson Imaging* **17**, 147–152.

Sund M, Xie L & Kalluri R (2004). The contribution of vascular basement membranes and extracellular matrix to the mechanics of tumor angiogenesis. *APMIS* **112**, 450–462.

Takuma S, Suehiro K, Cardinale C, Hozumi T, Yano H, Shimizu J, Mullis-Jansson S, Sciacca R, Wang J, Burkhoff D, Di Tullio MR & Homma S (2001). Anesthetic inhibition in ischemic and nonischemic murine heart: comparison with conscious echocardiographic approach. *Am J Physiol Heart Circ Physiol* **280**, H2364–H2370.

Taxt T, Jirik R, Rygh CB, Grüner R, Bartos M, Andersen E, Curry FR & Reed RK (2012). Single-channel blind estimation of arterial input function and tissue impulse response in DCE-MRI. *IEEE Trans Biomed Eng* **59**, 1012–1021.

Tofts PS (1997). Modeling tracer kinetics in dynamic Gd-DTPA MR imaging. *J Magn Reson Imaging* **7**, 91–101.

Tofts PS, Brix G, Buckley DL, Evelhoch JL, Henderson E, Knopp MV, Larsson HB, Lee TY, Mayr NA, Parker GJ, Port RE, Taylor J & Weisskoff RM (1999). Estimating kinetic parameters from dynamic contrast-enhanced T_1-weighted MRI of a diffusable tracer: standardized quantities and symbols. *J Magn Reson Imaging* **10**, 223–232.

Tomono Y, Naito I, Ando K, Yonezawa T, Sado Y, Hirakawa S, Arata J, Okigaki T & Ninomiya Y (2002). Epitope-defined monoclonal antibodies against multiplexin collagens demonstrate that type XV and XVIII collagens are expressed in specialized basement membranes. *Cell Struct Funct* **27**, 9–20.

Utriainen A, Sormunen R, Kettunen M, Carvalhaes LS, Sajanti E, Eklund L, Kauppinen R, Kitten GT & Pihlajaniemi T (2004). Structurally altered basement membranes and hydrocephalus in a type XVIII collagen deficient mouse line. *Hum Mol Genet* **13**, 2089–2099.

Wang P, Ba ZF, Burkhardt J & Chaudry IH (1993). Trauma-hemorrhage and resuscitation in the mouse: effects on cardiac output and organ blood flow. *Am J Physiol Heart Circ Physiol* **264**, H1166–H1173.

Additional information

Competing interests

Torfinn Taxt has a small stockholding in NordicNeuroLab AS that developed and manufactures the nICE software, which was used to create signal intensity curves for the step–slope model.

Author contributions

G.L, C.B.R and T.P. performed the animal experiments with MRI recordings. G.L. and C.B.R. did the subsequent analysis of the MR data using the step–slope-model. T.T. performed the analysis of data with aaJW method. R.H., R.S. and T. Pihlajaniemi provided the genetically modified mice, performed the histology and the analysis of the morphological data together with C.B.R. O.T. participated in planning the experiments and writing the manuscript. C.B.R., G.L, R.H., F.E.C. and R.K.R. planned the experiments, performed data analysis and wrote the manuscript. All co-authors have contributed to writing the manuscript and revising the paper.

Funding

The work was supported by the Research Council of Norway; the Regional Health Board of Western Norway; the Health Science Council of the Academy of Finland (grants 138866 and 128259 and Centre of Excellence 2012–2017 grant 251314) and the Sigrid Jusélius Foundation.

Acknowledgements

We acknowledge Gerd Salvesen and Jaana Peters for excellent technical assistance. The MR imaging was performed using the MR facility at MIC (Molecular Imaging Centre) at the University of Bergen. Staff at the electron microscopy core facility within the Tissue Imaging Center at Biocenter-Oulu are acknowledged for their assistance and expertise.